Integrated unmanned aerial vehicle platform with sensing and sampling systems for the measurement of air pollutant concentrations

Chen-Wei Liang [1,2], Chang-Hung Shen [1]

[1] Master Program in UAV Application and Smart Agriculture, National Ilan University, Yilan, Taiwan.

[2] Department of Biomechatronic Engineering, National Ilan University, Yilan, Taiwan.

Correspondence: Chen-Wei Liang (cwliang@niu.edu.tw)

Abstract

In this study, an unmanned aerial vehicle (UAV) platform with sensing and sampling systems was developed for three-dimensional (3D) measurements of air pollutant concentrations. The sensing system of this platform contains multiple microsensors and Internet of Things devices for determining the 3D distributions of four critical air pollutants and two meteorological parameters in real time. Moreover, the sampling system comprises remote-controllable gas sampling kits, each of which contains a Tedlar bag of 1 L for the 3D measurement of volatile organic compound concentrations according to the TO-15 method of the US Environmental Protection Agency. The performance of the developed UAV platform was verified in experiments where it was used to detect air pollutant emissions from a large industrial zone in Taiwan that included a traditional industrial park, a precision machinery park, and a municipal waste incineration plant. Three locations were selected as field measurement sites according to the prevailing local wind direction. The vertical distributions of four critical air pollutants, ambient temperature, and relative humidity were determined from data gathered at the aforementioned sites in March and May 2023. A total of 56 and 72 chemical species were qualitatively and quantitatively analyzed in these two periods, respectively. The experimental results verified the feasibility of using the proposed UAV platform for accurately evaluating the air pollutant concentration distribution and transport in an industrial zone. The sampling system can be used as a sampling part of the Method To-15, thus extending the method to measure the 3D distribution of VOCs in an area. The UAV platform can serve as a useful tool in the management and decision-making process of air pollution in industrial areas.

Keywords: Remote sensing, Low-altitude sampling, EPA method TO-15, Atmospheric monitoring, Vertical profiles, Low-cost microsensors, Particulate matter, Volatile organic compounds

1 Introduction

Unmanned aerial vehicle (UAV) remote sensing technology has been widely used in a variety of fields, such as defense, agricultural monitoring, surveying and mapping management, and disaster emergency response management (Yang et al., 2022), especially in the defence field (Zhu ey al., 2021). This technology is also used in environmental monitoring to determine the distributions of pollutants, especially air pollutants (Liu et al., 2020; Zheng et al., 2021; Shen et al., 2022; Sun et al., 2023). Fumian et al. (2021) used an UAV platform with metal oxide and photo-ionization detectors to confirm the presence of specific classes of chemicals in a contaminated area. UAV systems for air quality monitoring are inexpensive and allow for high-spatiotemporal-resolution data on air pollutant concentrations to be gathered over a large area (Gu et al., 2018). Cozma et al. (2022) proposed an autonomous multirotor aerial platform for the real-time, high-resolution monitoring of air quality in large cities by the obtained fine-grained heat-maps. Duangsuwan et al. (2022) used a UAV system capable of real-time air pollution monitoring and a machine learning method to obtain a three-dimensional (3D) air quality index (AQI) map of an area. Samad et al. (2022) developed a low-cost, practical, and reliable UAV system for the high-resolution 3D profiling of air pollutants at a roadside area. Galle et al. (2021) used a multirotor UAV to obtain in-situ measurements of sulfur dioxide (SO_2), hydrogen sulfide (H_2S), and carbon dioxide (CO_2) concentrations in volcanic gas plumes. De Fazio et al. (2022) developed a remote-controlled UAV with a wide set of sensors to measure the concentrations of air pollutants emitted by waste fires. Samad et al. (2022) developed a UAV system for the 3D profiling of particulate matter (PM), ultrafine particle, and black carbon concentrations. Suroto et al. (2018) designed a waypoint UAV for automatically determining the ambient carbon monoxide (CO) and PM concentrations. Arroyo et al. (2022) developed an electrochemical gas sensing module for a UAV to measure ambient CO, ozone (O_3), nitrogen monoxide (NO), and nitrogen dioxide (NO_2) concentrations. Yungaicela-Naula et al. (2017) used a UAV system and metaheuristic algorithms to measure air pollutant concentrations and track pollution sources in real time. Huang et al. (2022) integrated a UAV platform with an X-ray fluorescence analyzer to develop a high-efficiency system for the rapid detection of heavy metal pollution in soil.

UAV remote sensing technology has also been widely used in industrial safety management and agricultural production. Qiu et al. (2017) used a UAV-based monitoring platform and an artificial neural network model to conduct atmospheric dispersion simulation for identifying contaminant sources in a chemical industry park. Xie et al. (2013) proposed a design framework for an emergency atmospheric monitoring system based on a UAV platform. Their platform has high efficiency, high flexibility, and a wide monitoring range. Alvarado et al. (2015) developed a low-cost airborne sensing system based on a UAV platform for monitoring dust particles after blasting at open-pit mine sites. Rotorcraft UAVs are often used to spray pesticides, and the crop movement caused by the rotor of a UAV is a crucial indicator of the effectiveness of the spraying (2023). Boursianis et al. (2022) analyzed the roles of UAV and Internet of Things (IoT) technologies in irrigation, fertilizer application, pesticide application, weed management, plant growth monitoring, crop disease management, and field-level phenotyping. Their results indicated that UAV and IoT technologies are two of the most important technologies for transforming traditional farming practices into precision agriculture practices. Singh and Sharma (2022) proposed a platform for managing the agricultural crop information collected by a UAV, which has a high potential for use in agricultural applications such as crop health monitoring, fertilizer spraying, and pesticide spraying. In addition, UAV with low-cost Lidar sensor networks can provide continuous area surveillance of large spaces (Fumian et al., 2020). The UAV with sampling system can collect important samples for subsequent laboratory analysis and confirm results previously obtained from field measurements (Leitner et. al., 2023). Opportunities to collect samples of environmental contaminants expand the possibility of confirming field measurements through laboratory analysis (Pounds et al., 2011).

Most UAV environmental monitoring systems used in previous studies have contained various microsensors for measuring air pollutant concentrations. Few studies have proposed designs of UAV-based atmospheric sampling systems for the qualitative and quantitative analysis of low-altitude gas samples. The components of atmospheric gas samples, especially volatile organic compounds (VOCs), can be accurately identified and quantified through a combination of atmospheric sampling and laboratory analysis. In the present study, a UAV platform with sensing and sampling systems was developed for the measurement of low-altitude air pollutant concentrations. The developed UAV platform contains an atmospheric sensing system with various low-cost microsensors for the in-situ measurements of meteorological parameters and air pollutant concentrations to obtain their vertical profiles. Moreover, this platform contains a gas sampling system with multiple remote-controllable gas sampling sets. The gas samples collected by the gas sampling system were analyzed in a laboratory through gas chromatography–mass spectrometry (GC–MS) by using thermal adsorption equipment in accordance with the TO-15 method of the US Environmental Protection Agency (EPA). Finally, the developed UAV platform was verified in field experiments where it collected measurements in a large industrial zone, which included two industrial parks and a municipal waste incineration plant; these measurements were used to determine pollution levels and contamination sources.

2 Materials and methodology

2.1 Developed UAV platform

Figure 1 shows the prototype of the developed UAV platform, which comprises three parts: a UAV, a sensing system, and a sampling system. The hardware of the platform was constructed using off-the-shelf consumer parts, and the open-source software Ardupilot was used for flight control and data fusion. An all-in-one drone remote control solution for long-range, high-definition video transmission, namely Skydroid H16, was used as the UAV’s remote controller. The Pixhawk 6C Flight Controller was used as the autopilot, and the NEO V2 GPS module was used as the unmanned system positioning and navigation module because of its high sensitivity and strong resistance to interference. This module allows for an exact 3D spatial location of the sampling site to better describe the air quality of large spaces.

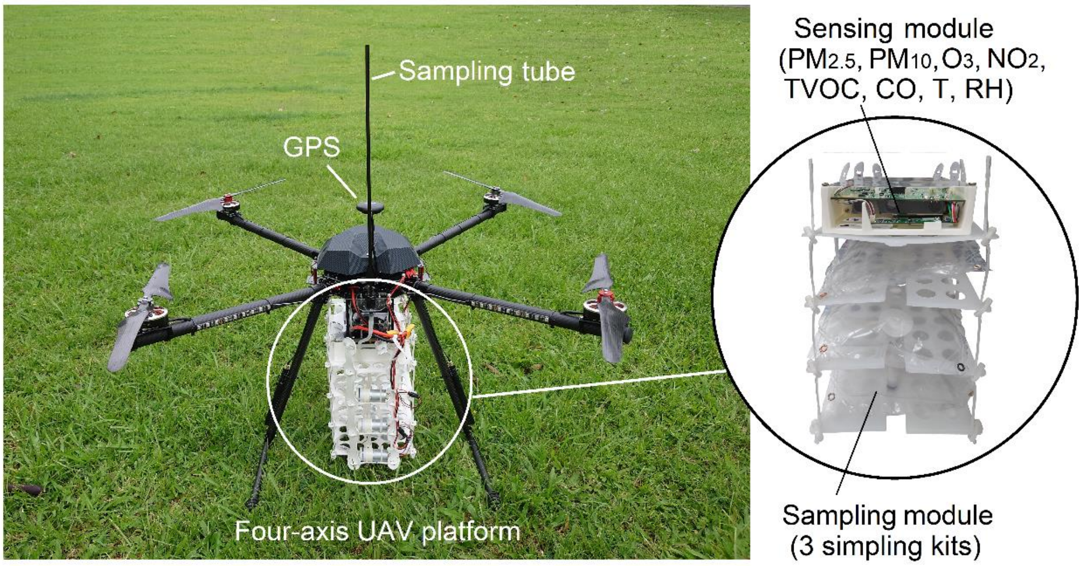

Figure1. Prototype of the UAV-based air sensing and air sampling systems.

2.2 Sensing system

The use of low-cost microsensors in a UAV platform offers numerous advantages for the measurement, especially real-time measurement, of the spatiotemporal distribution of air pollutant concentrations (Gu and Jia, 2019; Pochwała et al., 2020). The present study used a low-cost air quality monitoring kit (Air Quality Detector II, VISION) as the sensing system in the developed UAV platform. This monitoring kit is one of the air quality monitor sensors recommended by the Taiwanese Environmental Protection Administration. The parameters monitored with the aforementioned kit include $PM_{2.5}$ concentration, PM_{10} concentration, total VOC (TVOC) concentration, O_3 concentration, CO concentration, ambient temperature (T) and relative humidity (RH). The sensing system of the developed UAV platform is connected to an IoT system and a cloud server through a communication module to track air pollutant concentrations and weather data in real time. The data obtained by the microsensors of the sensing system are processed by a microprocessor, and the processed data are transferred to a cloud server for storage through Wi-Fi. The data stored on the cloud server can be presented in a graphical form in real time. The specifications of the sensing system are listed in Table 1.

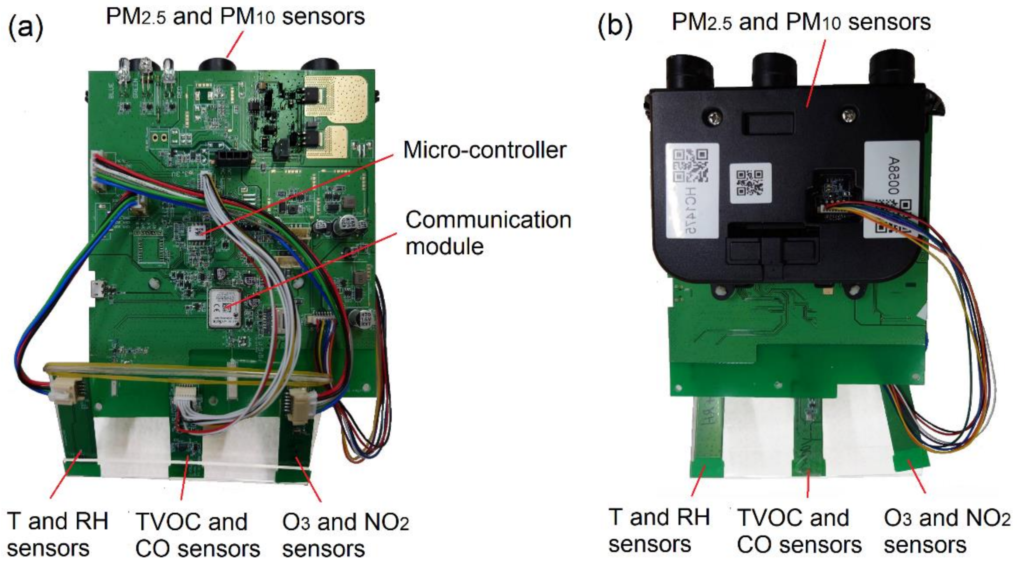

Figure 2. Circuit board with particulate matter and gas sensors used in the UAV platform. (a) front and (b) back of the circuit board.

Table 1. Specifications of sensing module

Sensors/devices	Measurement technique/principle	Label/model	Measurement range
T, °C	Bead thermistor	AMS/ENS210	–40 ~ +125
RH, %	Capacitive	AMS/ENS210	0 ~ 100
$PM_{2.5}$/PM_{10}, μg/m^3	Light scattering	VISION/AQ1001	1 ~ 1000
TVOC, ppb	Micro-hot plate technology	AMS/CCS811	0 ~ 29,206
O_3, ppb	Metal oxide chemiresistor	Renesas/ZMOD4510	20 ~ 500
NO_2, ppb	Metal oxide chemiresistor	Renesas/ZMOD4510	20 ~ 500
CO, ppm	Metal oxide chemiresistor	SGX/MiCS-5524	0.3 ~ 200
Communication module	–	Telit/ME310G1-WW	–
Micro-controller	–	Nuvoton/M481LIDAE	–

Prior to each field measurement run, the $PM_{2.5}$, PM_{10}, O_3, NO_2, TVOC, CO, T, and RH sensors had to be calibrated using monitoring data from the Wenshan Air Quality Monitoring Station of the Taichung City Environmental Protection Bureau (this station is located in the study area; Fig. 4).

2.3 Sampling system

The sampling module contains three gas sampling kits that each comprise three mini air pumps (TCS Electrical Co. JQC24381), a 1-L Tedlar bag (Keika Ventures), and a plastic one-way check valve with a compression spring (AliExpress, hose size: 4 mm). This one-way valve was installed in reverse to act as a pressure damper for the Tedlar bag after sampling by compression spring. Figure 3 shows the scheme of the sampling kit. The three air pumps of the sampling kits are connected in parallel to a length of 60-cm vertical sampling tube at the top of the UAV. The sampling kits are powered by the batteries of the UAV platform and are individually controlled by the UAV's remote controller. Therefore, the sampling system can perform multipoint sampling at different altitudes or locations in a single flight mission. Multipoint sampling in a single flight can overcome the problem caused by rapidly changing wind fields and makes it easier to obtain representative samples.

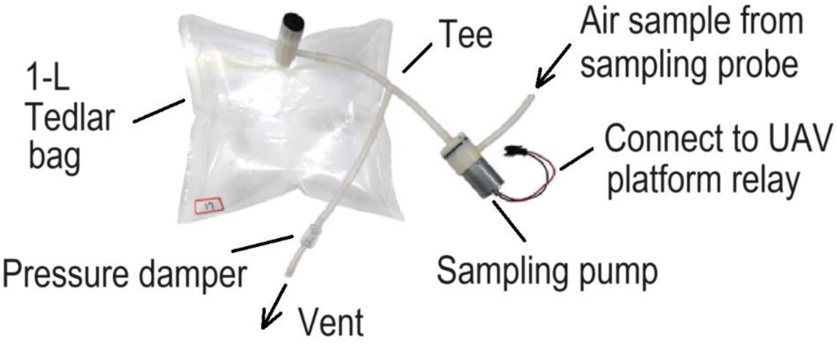

Figure 3. Scheme of the sampling kit.

2.4 Analysis of high-altitude VOC concentrations

The collected gas samples were analyzed in a laboratory in accordance with the TO-15 method of the US EPA. This method is based on criteria for the sampling and analysis of VOC in air and is primarily employed for the monitoring of airborne pollutants in urban and industrial environments. In the TO-15 method, air samples are collected in a special canister. Stainless-steel canisters are too heavy and bulky and thus are unsuitable for use in the developed UAV platform. Therefore, a 1-L Tedlar bag is used instead of a stainless-steel canister in the developed UAV platform. Ambient VOCs were collected in a 1-L Tedlar bag and analyzed by using GC–MS (Shimadzu QP-2010 SE GCMS) and thermal adsorption equipment (ENTECH 7100A Preconcentrator) in accordance with the analytical procedure of the TO-15 method. The analysis column in GC/MS was a Chrompack DB-1 capillary column with an inner diameter of 0.25 mm and a length of 60 m. In quantification of VOC species, 101 standard curves were prepared using the standard gases adopted in the calibration mixture of the TO-14A method of the US EPA, the ozone precursor mixtures adopted in the TO-15 method. Because these standard curves did not encompass all the compounds in the air samples, a semiquantitative method of analysis was used in which the analyte quantity was based on the standard curve of toluene (in the unit of parts per billion of toluene). Finally, all VOC concentrations were converted to the unit of parts per billion of carbon (ppbC). Because Tedlar bags are not as suitable as canisters for storing samples over long periods (more than approximately 30 days), the collected samples were analyzed within 10 days after sampling.

2.5 Field measurements

We used the developed UAV platform for detecting air pollutant concentrations in a large special industrial zone that included a traditional industrial park, a precision machinery park, and a municipal waste incineration plant. Figure 4 shows the location of the study area, which is located at the southern piedmont of the Dadu Tableland in the western part of the Taichung Basin, Taiwan. Two industrial parks [the Taichung Industrial Park (TIP) and the Taichung Precision Machinery Park (TPMP)], a municipal waste incineration plant [the Wenshan Waste Incineration Plant (WWIP)], and a landfill (the Wenshan Landfill) were located within the study area. The TIP is a large industrial space with a total area of 5.82 km^2. Currently, 1086 factories that employ a total of approximately 44 000 people are located in this industrial park. In addition to traditional industries, high-tech industries, such as optoelectronics, electronics, and precision machinery industries, are located in TIP. TPMP is an industrial park with an area of 1.61 km^2 and mainly includes companies focusing on precision machinery innovation. This industrial park is a crucial base of production of Taiwan’s machinery industry and has a land sales rate of 100%. As of the end of December 2022, 170 manufacturers that employ approximately 21 329 people operate in TPMP. WWIP began operation in 1995 and was the first large-scale incineration plant to be established in central Taiwan. This plant covers an area of 0.044 km^2 and has three incinerators that handle a total of 900 tons of waste per day. The Wenshan Landfill was opened in 1983 and covers an area of 0.365 km^2. The restoration of this landfill was completed in March 2019 and involved the installation of a solar photovoltaic system with a capacity of approximately 6.2 MWp on an area covering 0.0483 km^2. In addition, a busy national freeway and provincial expressway were located in the eastern part of the study area (Fig. 4) with weekday southbound and northbound traffic volumes of approximately 112 150 and 85 480 PCU, respectively.

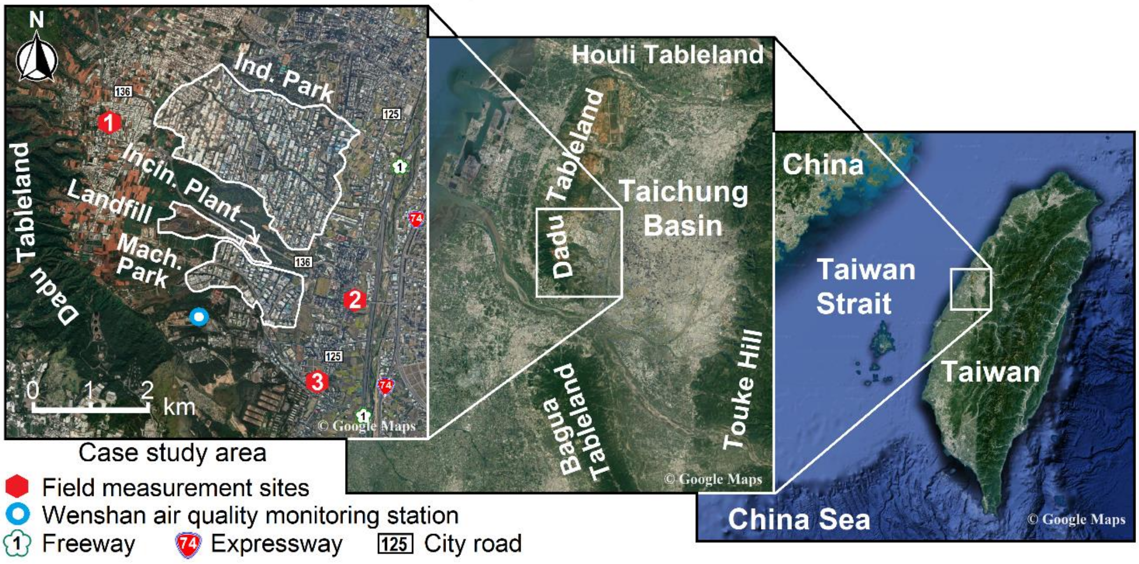

Figure 4. Locations of field measurement sites and Wenshan air quality monitoring station in the case study area.

The annual prevailing wind directions in the study area are north and north–northeast, which can be attributed to the spoon-shaped topography of the Dadu Tableland (Fig. 5). Moreover, the most prevalent local average wind speed is 1–3 m s^{-1}, followed by 3–5 m s^{-1}. Therefore, three locations were selected as field measurement sites (sites 1, 2, and 3) according to the prevailing wind directions (Fig. 5). These sites were located in densely populated parts of the study area. Site 1 was located upwind of the two industrial areas and WWIP, whereas sites 2 and 3 were located downwind of these areas and WMWIP. Because of regulations limiting the altitude of local flights to 200 ft (61 m), the heights at which samples were gathered were 2, 20, 40, and 60 m above the ground at each site. Noori and Dahnil (2020) indicated that a UAV monitoring system can accurately measure the concentrations of air pollutants at flight speeds slower than 6 m s^{-1} and that detection accuracy decreases considerably at flight speeds greater than 8 m s^{-1}. Therefore, the flight speed of the developed UAV platform was controlled at ≤6 m s^{-1} in this study.

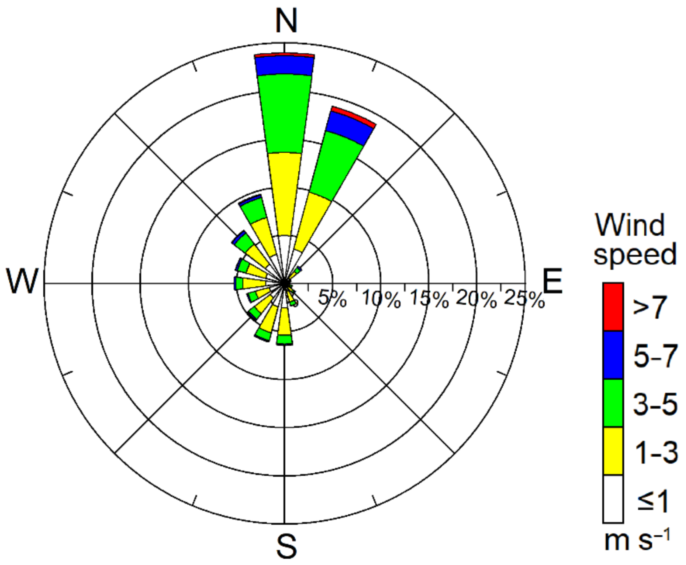

Figure 5. Annual wind rose of 2022 at the Wenshan air quality monitoring station.

2.6 Measurement of the speed and direction of the upper winds

To avoid the airflow caused by the rotor of the UAV from affecting the measurement of the speed and direction of the upper winds, the single-theodolite method was used in this study. A theodolite (WORLD E105-S Theodolite) was used to measure the speed and direction of the upper winds according to the pilot-balloon observation method (Pollak and Brunt, 1939). Figure 6 shows a schematic of the measurement of the upper winds by using the single-theodolite method, with Figs. 6(a) and 6(b) displaying the ground-projection-based and sliding-rule-based wind field diagrams, respectively. The formula for computing the speed of the upper winds is as follows:

$$u = 72L^{0.63}/(L+W)^{0.42} \tag{1}$$

$$r_1 = Z_1 \cot H_1 \tag{2}$$

$$V_e = Z_2 \cot H_2 \sin A_2 - Z_1 \cot H_1 \sin A_1 \tag{3}$$

$$V_n = Z_2 \cot H_2 \cos A_2 - Z_1 \cot H_1 \cos A_1 \tag{4}$$

$$\theta = \tan^{-1}(V_e/V_n) \tag{5}$$

$$P'Q' = V_e/\sin\theta \tag{6}$$

$$V = P'Q'/t \tag{7}$$

where u, L, and W are the rising speed (m/s), buoyancy (g), and weight of the pilot balloon (g), respectively; r_1, Z_1, and H_1 are the projected length (m) from the ground up to point p, the rising height (m), and the elevation angle (°), respectively; V_e and V_n are the eastern and northern projection lengths (m) of the wind speed, respectively; θ, A_i, and V are the northeastern wind speed angle (°), azimuth angle (°), and average wind speed at time t, respectively; and $P'Q'$ is PQ at ground projection (m). The wind directions at $P'Q'$ in quadrants I, II, III, and IV are defined to be 180° + θ, 180° – θ, θ, and 360° – θ, respectively.

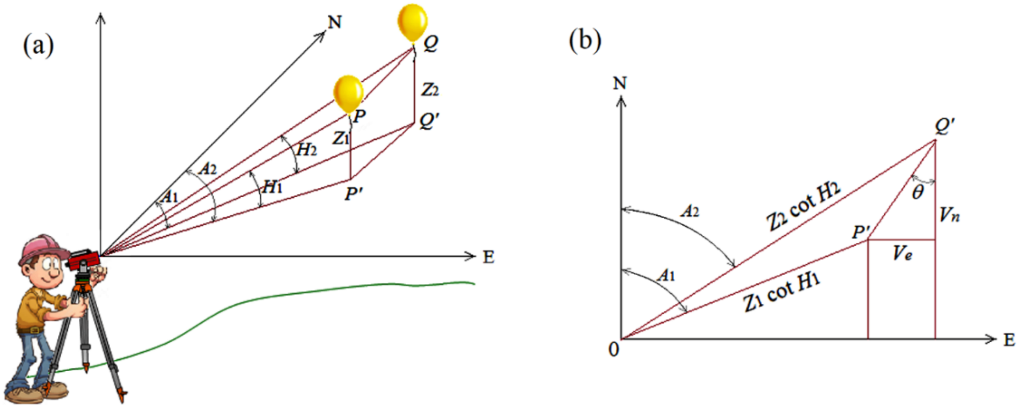

Figure 6. (a) geometry of the single-theodolite method and (b) the slide-rule method of computation.

3 Results and discussion

3.1 Field measurement 1

3.1.1 Upper winds

Figure 7 illustrates the observation results for the upper winds at the three field measurement sites between 13:30 and 16:30 on 29 March 2023. During the observation period, all wind directions at the three sites were between the north and northeast. All upper wind speeds observed at the three sites were less than 2 m s^{-1}. The prevailing wind directions at sites 1, 2, and 3 were north–northeast, north by east, and northeast, respectively. The wind speed at site 3 on the southern (downwind) side was marginally higher than those at the other two sites. The wind speeds at the three sites increased with altitude, which is consistent with the power law of the vertical distribution of wind speed. In the Taichung Basin, the average hourly wind speed was mostly between 0 and 3 m s^{-1}. The sampling period coincided with a period of comfortable weather in Taiwan.

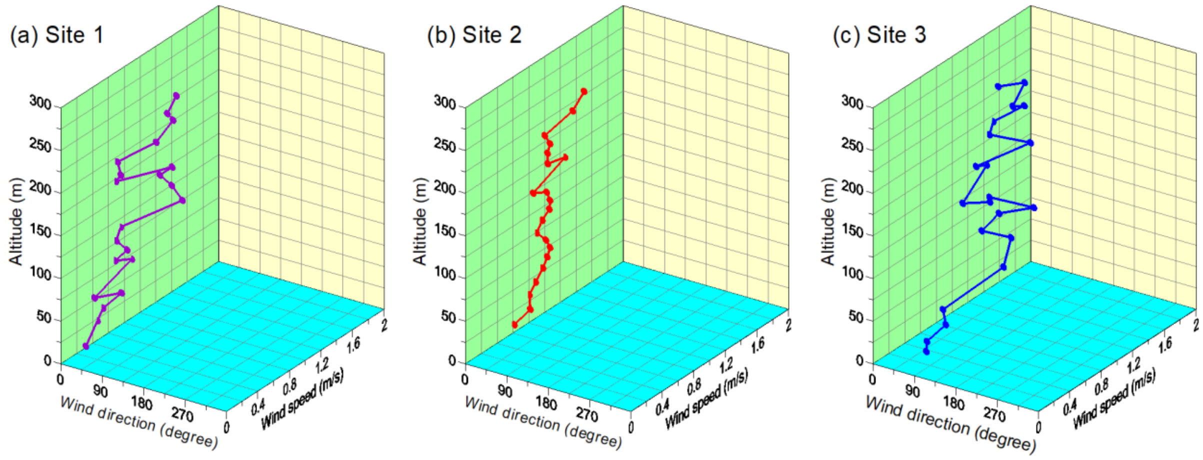

Figure 7. The observation results of upper winds during 13:30–16:30 on 29 March 2023, (a)–(c) are at sites 1–3, respectively.

3.1.2 Vertical distributions of critical air pollutants

Prior to each UAV telemetry run, the sensing system was connected to the IoT system to ensure that the monitoring data were input to the cloud server. Two runs were conducted at each monitoring site; thus, six runs were performed in total. Figure 7 displays the vertical distributions of critical air pollutants, ambient temperature, and RH during 13:30–16:30 on 29 March 2023. In Fig. 8, the solid and dashed lines represent the results obtained in runs 1 and 2 at each site, respectively. The PM$_{2.5}$ and PM$_{10}$ concentrations at the three sites were 11.0–17.3 (average = 13.4) and 11.9–19.3 (average = 15.0), respectively. The highest and lowest concentrations of PM (both PM$_{2.5}$ and PM$_{10}$) were observed at sites 2 (downwind) and 1 (upwind), respectively. The results indicate that the investigated industrial zone had high local PM concentrations, especially at site 2. CO is mainly emitted from mobile sources. Although the CO concentrations at the three sites were marginally variable but low. Therefore, the differences in the influences of the mobile source on the three locations were small. The TVOC concentrations at the three sites were very low (≤0.02 ppm), which might be attributable to the lack of large VOC emission sources in the investigated industrial zone. Because the sensitivities of the O$_3$ and NO$_2$ sensors were too low (Table 1), their monitoring data were 0 ppm in all the measurements.

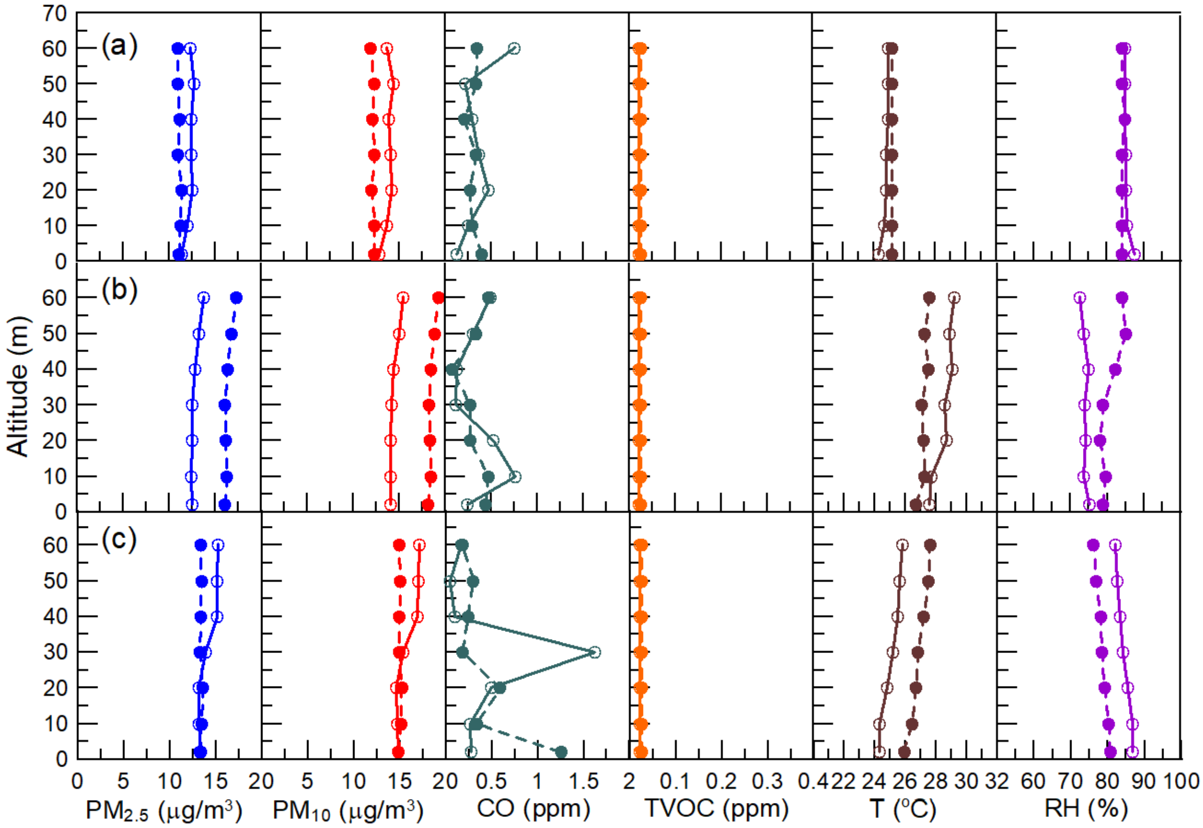

Figure 8. The observation results of critical air pollutants, ambient temperature, and relative humidity during 13:30–16:30 on 29 March 2023, (a)–(c) are at Sites 1–3, respectively. Solid and dashed lines are the results of Run 1 and Run 2, respectively.

The temperature ranges at sites 1 to 3 were 24.3–25.2 °C (average = 25.0 °C), 26.7–29.2 °C (average = 27.9 °C), and 24.3–27.6 °C (average = 26.0 °C). At all locations, the lowest temperature was observed at the ground because of the heat radiation from the surface on cloudy days. The temperatures at the three sites gradually decreased in the afternoon with time. The RH values of the three locations changed with the temperature, and the RH range in the study area was 76.1%–87.6%.

3.2.3 Vertical distributions of VOCs

Sampling was performed twice at four altitudes at each site by using the UAV platform; thus, eight samples were collected per site. Figure 9 displays the analysis results obtained through GC–MS with thermal adsorption equipment for the upper-altitude VOCs at the three sites during 13:30–16:30 on 29 March 2023, using GC–MS. A total number of more than 56 species were analyzed at different altitudes at the each site. The analysis results indicated the feasibility of using the developed UAV platform with a Tedlar bag sampling system for the 3D measurement of VOC concentrations in accordance with the TO-15 method. All dominant VOCs at various altitudes at the three sites appeared within the retention time of 10–15 min in GC-MS chromatography. The peak pattens of the dominant species at the three sites were highly similar, which indicated that the three sites had similar air pollution sources. A second set of dominant VOCs appeared at various altitudes within the retention time of 17–24 min, especially at site 3. The second dominant species at site 2 had a considerably higher concentration than did those at the other sites, which indicated that site 2 was located downwind of some air-pollution emission sources. TIP is located upwind of site 2 (Fig. 4).

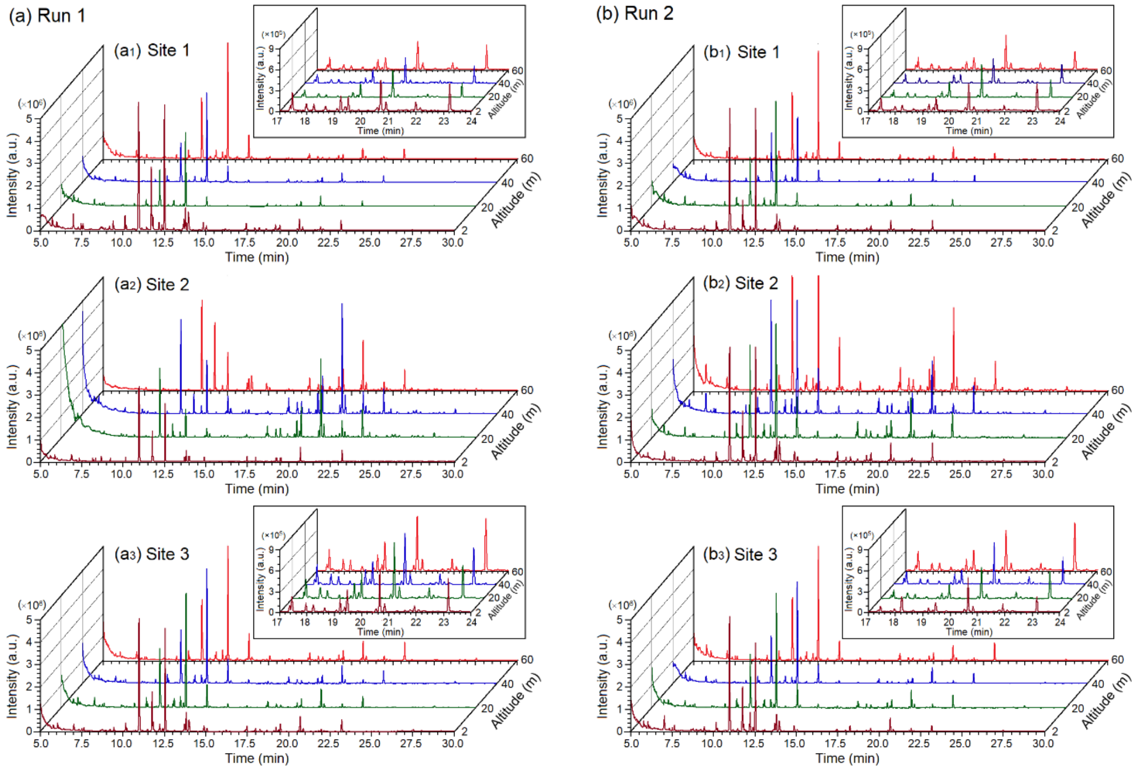

Fig. 9. The analysis results of upper-altitude VOCs during 13:30–16:30 on 29 March 2023. (a) and (b) show the results of run 1 and run 2, respectively. The insets in each subfigure are zoomed-in views over the retention time range from 17 to 24 minutes.

Table 2 lists the qualitative and quantitative analysis results of the VOC samples collected from the three sites, where the concentration is the average of those obtained in two sampling runs (runs 1 and 2 in Fig. 9). The concentrations of the top five VOC species at the four sampled altitudes had the following order from highest to lowest: site 1, toluene > 2,4-dimethyl heptane > 4-methyl octane > propyl propionate > 3,7-dimethyl undecane; site 2, 2,4-dimethyl heptane > toluene > 4-methyl octane

> 3,7-dimethyl undecane > propyl propionate; and site 3, 2,4-dimethyl heptane > toluene > 4-methyl octane > propyl propionate > 3,7-dimethyl undecane. The ranges of the concentration ratio of the top five species to all upper-altitude VOCs at sites 1, 2, and 3 were 71.1%–80.9% (average = 74.9%), 69.1%–79.7% (average = 72.9%), and 72.3%–76.8% (average = 73.6%), respectively. Thus, the top five VOC species dominated the upper-altitude VOC concentrations.

Table 2. The average concentrations (in ppbC) of upper-altitude VOCs at the three sites during March 29, 2023.

Species	Retention time (min)	Altitude at Site 1 (m)				Altitude at Site 2 (m)				Altitude at Site 3 (m)			
		2	20	40	60	2	20	40	60	2	20	40	60
Ethanol	5.70	1.8	2.3	1.4	1.2	0.6	2.9		5.1	1.7	1.2	1.7	2.0
Acetone	5.98	0.8	0.8	0.8	0.6	0.9	0.8	1.4	1.2	1.4	1.2	0.8	0.9
Isopropanol	6.11	0.6	0.9							0.6			
2-Methyl pentane	6.99	3.9	3.5	2.6	3.0	3.3	4.7	9.0	4.8	5.1	4.4	2.7	3.6
2-Butanone	7.29	0.3	0.3	0.3	0.3	0.2	0.2	0.3	0.2	0.3	0.3	0.3	0.3
Hexane	7.48	1.4	0.6	0.6	0.6	1.4	1.1	1.2	0.9	0.8	0.9	0.6	1.2
Ethyl Acetate	7.58	1.1	0.8	0.8	0.8	0.8	0.9	0.8	0.9	1.1	0.8	0.8	0.8
Benzene	8.59		0.2	0.2	0.2	0.5	0.8	0.9	1.1	0.3	0.5	0.5	0.3
1-Butanol	8.62	0.5			0.2					0.2			
2-Methyl hexane	8.73	0.3	0.5	0.3	0.2		0.3	0.5	0.5	0.2	0.3	0.3	0.3
Cyclohexane	8.91	0.5											
3-Methyl hexane	8.95	0.3	0.2	0.2	0.2	0.3	0.3	0.5	0.5	0.5		0.3	0.3
Pentanal	9.07	0.2	0.0	0.0	0.0					0.2		0.0	0.2
1,2-Dichloro propane	9.19	1.2				0.5				0.8			
Heptane	9.40	1.7	1.1	0.9	1.1	1.8	1.8	2.6	2.0	1.2	1.2	1.1	1.2
2,5-Dimethyl hexane	10.12	3.5	2.1	1.7	2.4	2.7	4.2	5.0	4.4	2.4	2.7	2.3	2.7
2,4-Dimethyl hexane	10.19	0.8	0.5	0.5	0.8	0.8	1.1	1.4	1.4	0.8	0.8	0.6	0.8
2,5-Dimethyl-1-hexene	10.58	0.2	0.0	0.0	0.0			0.2	0.0	0.0	0.0	0.0	0.0
2-Ethyl-1-butanol	10.70	0.5	0.3	0.3	0.5		0.5	0.5	0.5	0.3	0.5	0.3	0.5
Toluene	10.94	87.9	16.5	17.3	25.1	71.3	35.7	45.5	45.2	49.2	23.0	19.7	24.5
3-Methyl heptane	11.15	0.3	0.2	0.2	0.2		0.5	0.3	0.3	0.3	0.2	0.2	0.3
Hexanal	11.44	0.5	0.3	0.3	0.5	0.5	0.5	0.5	0.6	0.5	0.5	0.5	0.5
Propyl propionate	11.71	15.6	0.3	0.3	0.9	17.1	1.2	1.5	2.3	13.7	0.6	0.5	0.9
Octane	11.79	3.5	1.8	1.4	2.0	2.1	3.5	3.5	3.9	1.1	2.0	1.7	2.1
2,3,5-Trimethyl hexane	12.36	1.2	0.8	0.8	0.9	1.2	1.7	2.0	2.3	1.1	1.4	1.1	1.1
2,4-Dimethyl heptane	12.50	42.9	28.1	24.6	41.3	43.8	62.4	77.4	81.6	30.5	38.6	35.3	42.2
2,6-Dimethyl heptane	12.66	0.3	0.2	0.2	0.2	0.3		0.3	0.5		0.2	0.2	0.2
2,4-Dimethyl-1-heptene	13.06	0.2	0.2	0.2	0.2	0.3	0.3	0.3	0.3	0.2	0.2	0.2	0.2
3-Ethyl-2-methyl hexane	13.60	0.2	0.0	0.2	0.2		0.5	0.5	0.6	0.2	0.3	0.3	0.3
Ethyl benzene	13.68	3.0	0.0	0.2	0.2	3.9				2.4		0.3	0.3
4-Methyl octane	13.77	6.5	3.8	4.7	6.9	7.8	13.4	15.6	17.7	5.7	6.9	6.9	8.0
m-Xylene	13.94	10.4	0.5	0.6	1.2	14.7	2.3	2.1	2.9	7.8	0.9	1.2	1.5
o-Xylene	14.84	3.3		0.3	0.6	6.6	0.9	0.9	1.4	3.5	0.6	0.5	0.3
Nonane	15.03	1.1	0.5	0.6	0.8	1.5	2.0	2.7	3.2	0.8	1.1	1.1	1.2
2,4,6-trimethyl heptane	15.80							0.2	0.3				0.2
3,5-Dimethyl octane	16.04	0.2		0.0	0.2		0.3	0.3	0.5		0.2		0.2
2,7-Dimethyl octane	16.18	0.3	0.2	0.2	0.3	0.8	1.1	1.2	1.4	0.5	0.5	0.5	0.5
2,6-Dimethyl octane	16.40	0.2					0.3	0.5	0.5		0.2		0.2
2,5-Dimethyl octane	17.36	0.3	0.2	0.2	0.3	0.6	1.2	1.1	1.7	0.3	0.3	0.3	0.5
2-Methyl nonane	17.44	1.5	0.6	0.8	1.2	2.4	4.2	3.9	5.9	0.9	1.2	1.4	1.8
2,5-Dimethyl nonane	17.95	0.6	0.5	0.5	0.6	1.2	2.4	2.6	3.8	0.6	0.9	0.9	0.9
Decane	18.64	0.3	0.2	0.2	0.3	0.6	1.1	0.9	1.4	0.3	0.3	0.3	0.5
4-Methyl decane	19.07	0.2	0.2	0.2	0.2	0.2	0.5	0.8	1.2	0.2	0.2	0.2	0.2
Undecane	19.20	0.9	0.5	0.6	0.8	1.7	3.2	3.0	5.7	0.8	0.9	1.1	1.2
2,5,6-Trimethyl decane	19.36	0.3	0.2	0.2	0.2	0.3	0.9	0.8	1.5	0.3	0.3	0.3	0.3
4-Methyl-5-propyl nonane	19.47	1.1	1.1	0.8	0.9	1.8	3.9	4.7	7.5	1.2	1.5	1.4	2.0
Dodecane	20.53	0.3	0.2	0.2	0.2	0.3	0.8	1.2	1.7	0.3	0.3	0.3	0.5
3,7-Dimethyl undecane	20.65	2.4	2.6	2.1	2.6	4.4	9.2	12.8	19.1	3.2	3.5	3.8	3.9
4-Methyl-1-undecene	20.84	0.2	0.0	0.2	0.2	0.2	0.5	0.5	0.9	0.2	0.2	0.2	0.2
Undecanal	21.56			0.2			0.3	0.3	0.5			0.2	0.2
2,3-Dimethyl decane	21.77		0.2	0.2	0.2		0.5	0.6	0.9	0.2	0.2	0.2	0.2
Tridecane	21.93	0.5	0.3	0.2	0.5	0.8	1.5	2.1	2.7	0.5	0.6	0.6	0.8
2,3,5,8-Tetramethyl decane	22.09	0.2	0.0	0.2	0.2		0.5	0.6	0.9	0.2	0.2	0.2	0.2
2-Heptyl-1,3-dioxolane	22.27			1.5	1.5								
2-Methyl tridecane	23.59						0.3	0.5	0.6				0.0
2,6-Dimethyl undecane	24.00						0.2		0.5				
Total		204.8	72.9	69.5	102.3	199.5	176.1	214.8	244.2	143.3	101.7	92.6	111.9

Toluene and 2,4-dimethyl heptane exhibited the highest or second-highest concentrations among the VOCs at the three sites. Toluene might originate from vehicle exhaust and industrial emissions.

Common industrial organic solvents, such as benzene, xylene, ethylbenzene, and butanone, were detected at the four altitudes at each site, which indicated that a considerable quantity of the toluene in the study area originated from industrial emissions. In general, because its branched structure allows for combustion without knocking, 2,4-dimethyl heptane is blended with other gasoline components to produce high-octane fuel. In addition, alkanes were the dominant VOC species at various altitudes and sites. Thus, the concentrations of the VOCs originating from vehicle exhaust might have been higher than those of the VOCs originating from industrial exhaust. Propyl propionate is a safer alternative for toluene because of its low odor, moderately volatile nature, and nonhazardous and nonpolluting ester product; thus, the propyl propionate detected field measurement 1 mainly originated from industrial emissions. The average VOC concentrations at the three sites had the following order from highest to lowest: site 2 > (site 1 ≈ site 3). The highest and second-highest total VOC concentrations at sites 1 and 3 appeared at altitudes of 2 and 60 m, respectively. By contrast, the highest and second-highest total VOC concentrations at site 2 appeared at altitudes of 60 and 40 m, respectively. This result indicates that some VOCs were transmitted from upwind sources.

3.2 Field measurement 2

3.2.1 Upper winds

Figure 10 shows the observation results for the upper winds at the three field measurement sites between 13:30 and 16:30 on 10 May 2023. During the measurement period, all wind directions at the three sites were between north and east. The prevailing wind directions at sites 1, 2, and 3 were north–northeast, northeast by east, and northeast by east, respectively. The upper wind speeds at sites 1–3 were 1.1–5.6 m s^{-1} (average = 3.5 m s^{-1}), 1.2–5.1 m s^{-1} (average = 3.6 m s^{-1}), and 1.2–5.2 m s^{-1} (average = 3.7 m s^{-1}), respectively. The wind speeds at the three sites increased with an increase in altitude but decreased marginally as the altitude increased beyond 200 m. Compared with the upper winds during the field measurement 1 (on 29 March 2023), those during field measurement 2 (on 10 May 2023) had higher speed and a more easterly direction.

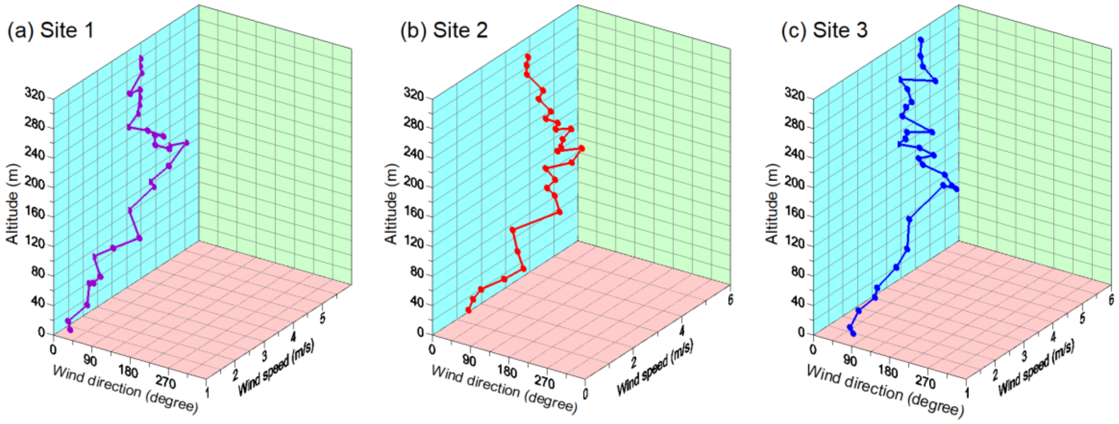

Figure 10. The observation results of upper winds during 13:30–16:30 on 10 May 2023.

3.2.2 Vertical distributions of critical air pollutants

As was the case in field measurement 1, two runs of UAV telemetry were implemented at each monitoring site; thus, a total of six runs were performed. The sensing system was connected to the

IoT system prior to UAV telemetry to ensure that the monitoring data were input to the cloud server after each run. Figure 11 displays the vertical distributions of critical air pollutants, ambient temperature, and RH for the period of 13:30–16:30, 10 May 2023. The $PM_{2.5}$ and PM_{10} concentration ranges at the three sites were 12.1–16.8 μg m^{-3} (average = 13.1 μg m^{-3}) and 13.1–17.4 μg m^{-3} (average = 14.3 μg m^{-3}), respectively. The highest and lowest concentrations of PM (both $PM_{2.5}$ and PM_{10}) were observed at sites 3 (downwind) and 2 (upwind), respectively. The highest CO concentrations at the three sites were at the ground level, and the highest CO concentration of 4.66 ppm was measured at site 2. The CO concentrations at all altitudes except for the ground level at the three sites varied between 0 and 2.4 ppm. As was the case in field measurement 1, the O_3 and NO_2 concentrations were 0 ppm in measurement 2 because the sensitivities of the O_3 and NO_2 sensors were too low. The TVOC concentrations at the three sites were very low (≤0.02 ppm; as in field measurement 1), possibly because the sensitivity of the TVOC sensor was too low.

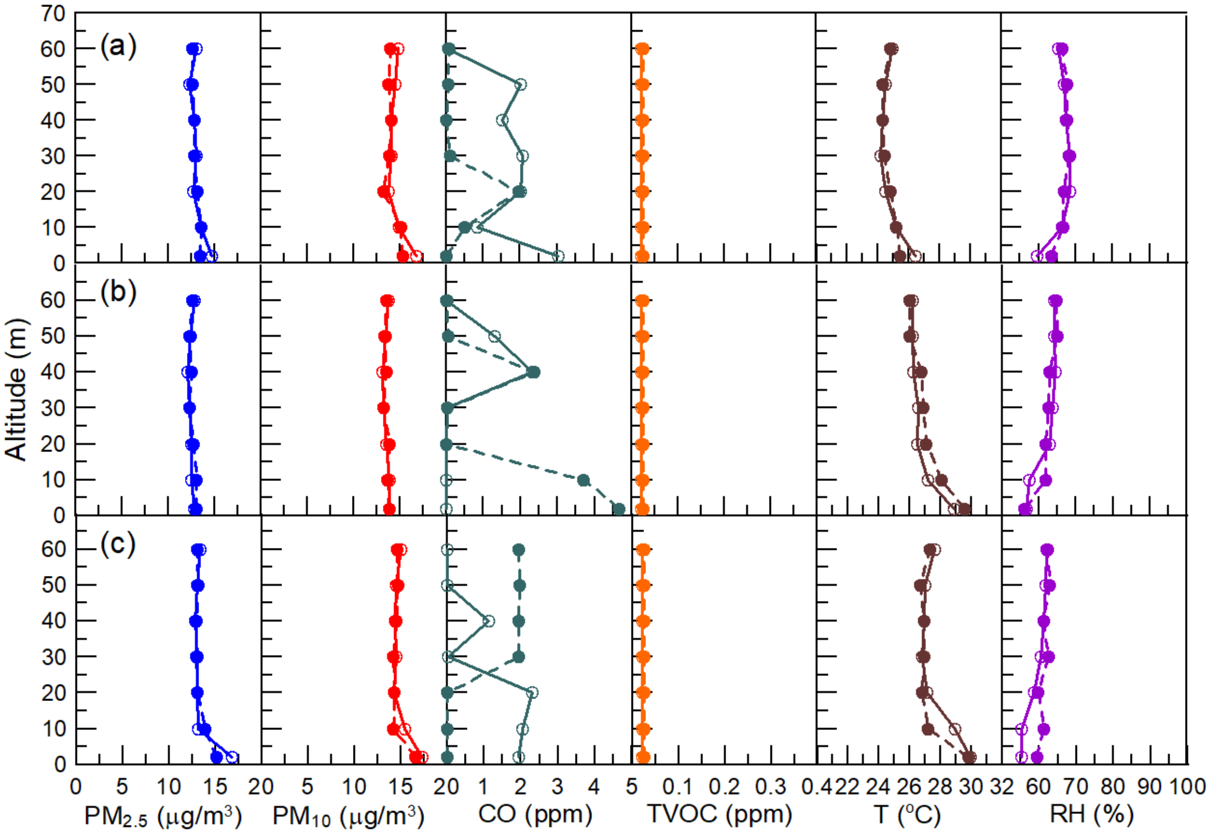

Figure 11. The observation results of critical air pollutants, ambient temperature, and relative humidity during 13:30–16:30 on 10 May 2023, (a)–(c) are at sites 1–3, respectively. Solid and dashed lines are the results of run 1 and run 2, respectively.

The temperature ranges at sites 1–3 were 24.12–26.4 °C (average = 24.9°C), 26.0–29.6 °C (average = 27.0 °C), and 26.7–29.9 °C (average = 27.6 °C), respectively. The highest temperatures at these sites were observed at the ground level because of the thermal radiation of the surface on sunny days. The temperatures at the three sites gradually decreased in the afternoon with time. The RH values of the three sites changed with the temperature, and the RH range in the study area was 55.1%–68.4%.

3.2.3 Vertical distributions of VOCs

Figure 12 depicts the GC–MS analysis results for upper-altitude VOCs at the three field measurement sites during 13:30−16:30 on 10 May 2023. Sampling was performed twice at four altitudes (2, 20, 40, and 60 m) at each site by using the UAV platform; thus, a total of 24 measurements were performed (eight at each site). A total of 79 VOCs species were analyzed at different altitudes at the three sites, and this number is higher than the number of VOCs analyzed in field measurement 1 (i.e., 52). All the dominant VOC species at various altitudes at the three sites appeared within the retention time of 10−15 min in GC–MS chromatogram, which is in line with the results obtained in field measurement 1. The peak pattens of the dominant VOC species at the three sites were highly similar, which indicated that the three sites had similar air pollution sources. The highest peak intensities of the dominant VOC species at the three locations were observed at an altitude of 2 m. A second dominant VOC species appeared at various altitudes within the retention time of 17–24 min, especially at an altitude of 60 m at site 1. The peak intensity of the second dominant species at site 2 was considerably lower than those at the other two sites. In addition, the concentrations of all the VOCs at an altitude of 60 m at site 2 were lower than those at the same altitude at sites 1 and 3.

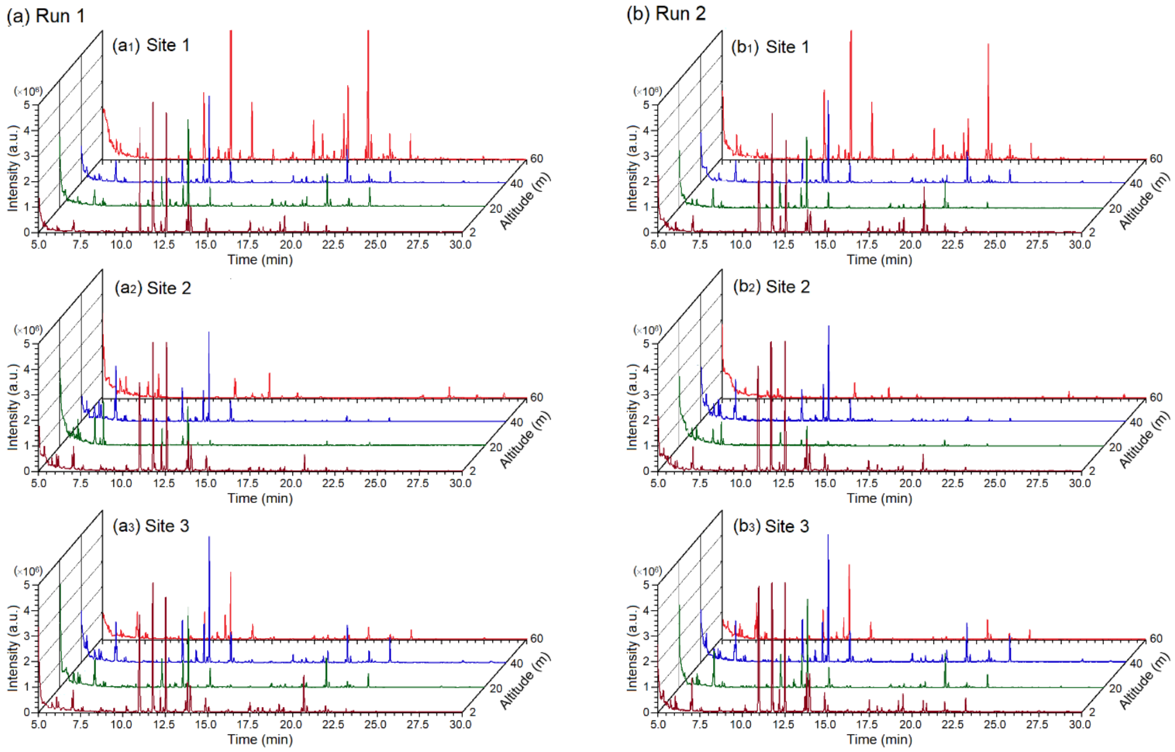

Figure 12. The analysis results of upper-altitude VOCs during 13:30−16:30 on 10 May 2023. (a) and (b) show the results of run 1 and run 2, respectively.

Table 3 lists the average upper-altitude VOC concentrations at the three sites on 10 May 2023. The total upper-altitude VOC concentrations at the three sites in field measurement 2 was marginally lower than that in field measurement 1; however, the total number of VOC's detected in field measurement 2 was higher than that in field measurement 1. In addition, the highest and lowest VOC concentrations occurred at an altitude of 2 m at site 3 and at an altitude of 60 m at site 1, respectively. This result is different to that obtained in field measurement 1.

Table 3. The average concentrations (in ppbC) of upper-altitude VOCs at the three sites during May 10, 2023.

Species	Retention time (min)	Altitude at Site 1 (m)				Altitude at Site 2 (m)				Altitude at Site 3 (m)			
		2	20	40	60	2	20	40	60	2	20	40	60
1-Butene	5.27	2.0	4.6	4.9		4.0	2.6	4.7	0.2	3.5	3.2	3.8	2.8
Ethylene oxide	5.58	2.1	1.4			2.2	2.7	2.6	2.2	2.2	1.6	0.7	0.3
Ethanol	5.73	0.7	1.0	1.4	2.5	1.7	2.1	3.8	1.8	2.7	3.5	2.9	1.9
Acetone	6.00	1.0	1.1	1.6	0.6	1.8	2.2	3.1	1.6	2.6	2.7	1.7	1.7
Isopropanol	6.11	0.8	0.9	1.1		3.1	1.3	5.8	0.6	1.9	4.2	3.1	1.9
Cyclobutanol	6.39	0.3	0.6	0.5	0.3	1.1	0.6	0.9	0.5	0.8	0.4	0.4	0.4
2-methyl-2-Propanol	6.48				1.7								
trimethyl Silanol	6.93	1.7				4.7		4.2		3.1	2.5	3.7	1.7
2-Methyl pentane	6.99	5.9	9.0	11.0	3.0	7.7	6.1	14.2	3.3	9.4	9.7	15.3	12.5
2-Butanone	7.29	0.2	0.3	0.3	0.2	0.3	0.6	0.4	0.3	0.3	0.4	0.4	0.4
Hexane	7.47	0.6	2.2	1.3	1.2	1.0	7.7	1.6	4.0	1.2	1.9	1.6	1.9
Ethyl Acetate	7.58	0.5	0.5	0.6	0.4	1.0	0.7	1.2	0.3	1.2	0.9	1.0	1.0
2-methyl-1-Propanol	7.92					0.2		0.3	0.1		0.2	0.2	0.1
Benzene	8.61		0.2			1.8	0.3	0.6	0.2	1.6	0.5	0.5	0.3
1-Butanol	8.66	0.6	0.2		0.4								
2-Methyl hexane	8.73	0.1	0.2		0.2	0.4	0.3	0.4	0.2	0.3	0.4	0.3	0.3
3-Methyl hexane	8.93	0.2	0.2		0.2	0.5	0.3	0.5	0.2	0.4	0.4	0.4	0.4
Pentanal	9.07	0.1	0.2		0.1	0.1	0.0	0.1		0.1	0.2	0.1	0.1
1-Heptene	9.13	0.1	0.1		0.0	0.1	0.0	0.1		0.1	0.1	0.1	0.1
2,2,4-trimethyl-Pentane	9.27				0.0	0.1	0.1		0.1				
Heptane	9.41	0.7	0.7	0.5	0.9	1.0	0.2	0.8	0.2	1.0	0.6	0.7	0.6
2,5-Dimethyl hexane	10.12	1.0	1.2	0.9	2.3	1.5	0.2	1.0	0.2	1.7	1.0	1.1	1.0
2,4-Dimethyl hexane	10.20	0.3	0.3	0.3	0.6	0.4	0.1	0.3	0.1	0.5	0.3	0.4	0.2
2-Ethyl-1-butanol	10.71	0.3	0.2		0.3	0.2	0.2	0.3		0.4	0.2	0.3	0.2
Toluene	10.94	41.0	9.4	8.0	18.7	52.3	3.7	11.0	4.1	55.9	10.0	12.9	9.7
3-Methyl heptane	11.14	0.2	0.1	0.1	0.2	0.2	0.1	0.2		0.3	0.2	0.2	0.2
Hexanal	11.42	0.6	1.1	0.4	0.4	0.6	0.2	0.4	0.1	0.4	0.5	0.5	0.5
Propyl propionate	11.71	50.6	0.5	0.6	0.3	74.4		1.4	0.6	64.9	1.1	2.7	1.7
Octane	11.80	0.8	0.7	0.6	2.5	1.0	0.1	0.7	0.1	1.2	0.7	0.6	0.4
Hexamethylcyclotrisiloxane	12.17	4.3	6.6	6.4	2.1	5.7	1.7	10.2	0.8	7.4	7.7	11.0	7.5
2,3,5-Trimethyl hexane	12.36	0.9	0.9	1.0	2.1	1.6	0.2	1.3	0.2	1.5	1.2	1.4	1.0
2,4-Dimethyl heptane	12.51	28.9	21.7	23.1	64.0	40.0	5.8	25.0	3.8	39.7	23.7	28.9	19.6
2,6-Dimethyl heptane	12.67	0.2	0.1		0.3	0.2		0.1		0.3	0.1	0.2	0.1
2,4-Dimethyl-1-heptene	13.06	0.2	0.2	0.2	0.6	0.2	0.1	0.1	0.1	0.2	0.2	0.2	0.1
3-Ethyl-2-methyl hexane	13.60	0.2	0.3	0.4	0.6	0.3	0.1	0.3	0.1	0.3	0.4	0.4	0.3
Ethylbenzene	13.67	3.3				3.4	0.1	0.2	0.2	4.4		0.4	0.2
4-Methyl octane	13.77	7.0	5.0	5.9	13.8	8.5	0.9	6.1	0.9	9.4	5.6	7.2	4.6
m-Xylene	13.94	14.7	0.7	0.7	0.5	15.6	0.3	1.6	0.5	20.3	1.0	2.5	1.0
3-ethyl-2,3-dimethyl Pentane	14.22	0.1	0.1		0.2	0.3	0.7	0.1				0.1	
1,3,5,7-Cyclooctatetraene	14.63	0.2	0.2		0.1	0.2	0.2	0.2				0.2	0.2
o-Xylene	14.84	7.5	0.3		0.3	8.8	0.2	0.5	0.5	9.5	0.5	1.1	0.5
Nonane	15.03	1.4	0.7	0.7	2.5	1.4	0.2	0.4	0.2	1.9	0.6	0.8	0.5
2,4,6-trimethyl heptane	15.78	0.1	0.0		0.2	0.1				0.1		0.1	
3,5-Dimethyl octane	16.05	0.2	0.1		0.5	0.3				0.3		0.1	
2,7-Dimethyl octane	16.18	0.6	0.3	0.3	1.6	0.7		0.2		0.8	0.2	0.3	0.2
2,6-Dimethyl octane	16.40	0.2	0.1		0.5	0.2				0.2		0.1	
2,5-Dimethyl octane	17.37	0.6	0.3	0.3	1.7	0.4		0.1		0.6	0.2	0.3	0.2
2-Methyl nonane	17.44	2.4	1.2	1.3	6.4	1.3	0.1	0.4	0.2	2.3	0.8	1.3	0.7
2,2,3,5-Tetramethyl heptane	17.53		0.2				0.1	0.1				0.2	0.1
6-Methyl-5-hepten-2-one	17.83		0.0	0.1	0.2		0.0	0.0	0.1	0.1	0.1	0.1	0.0
2,5-Dimethyl nonane	17.96	1.2	0.8	0.8	4.7	1.3	0.1	0.3	0.1	1.5	0.6	0.7	0.5
Octamethylcyclotetrasiloxane	18.21	1.4	0.9	1.0	0.7	0.5	0.1	0.2	0.1	0.9	0.6	0.9	0.7
Octanal	18.32	0.1	0.2	0.1	0.3							0.1	0.1
Decane	18.65	0.8	0.3	0.4	1.6	0.2		0.2	0.1	0.7	0.3	0.4	0.2
4-Methyl decane	19.07	0.4	0.2	0.2	1.5	0.1		0.1		0.4	0.2	0.2	0.1
Undecane	19.21	2.1	1.1	1.2	7.0	0.8	0.1	0.2	0.1	2.1	0.7	1.2	0.6
2,5,6-Trimethyl decane	19.37	0.7	0.3	0.2	2.0	0.2			0.1	0.6	0.2	0.3	0.2
4-Methyl-5-propyl nonane	19.47	3.1	1.6	1.6	9.7	0.8	0.1	0.3	0.3	2.2	1.2	1.7	0.8
2,3-Dimethyl decane	20.53	0.5	0.5	0.5	2.2	0.2	0.1	0.1	0.1	0.6	0.4	0.5	0.4
3,7-Dimethyl undecane	20.66	5.5	5.9	6.4	26.2	3.2	0.7	1.0	1.3	5.0	5.5	7.2	3.1
4-Methyl-1-undecene	20.85	0.4	0.3	0.4	1.0	0.1	0.0	0.1	0.1	0.4	0.3	0.4	0.2
7-Methyl-1-undecene	21.11	0.0	0.0	0.0	0.1	0.0				0.0	0.0	0.0	0.0
2-methyl-1-Decanol	21.30				0.5								
Undecanal	21.43	0.1	0.2	0.2	0.5					0.3	0.3	0.2	0.2
Dodecane	21.59	0.4	0.3	0.3	0.8	0.1		0.1		0.4	0.3	0.4	0.2
Tridecane	21.78	1.4	0.8	1.5	3.2	0.4	0.1	0.3	0.3	1.5	0.9	1.6	0.9
2,3,5,8-Tetramethyl decane	22.09	0.4	0.3	0.5	0.9	0.1	0.0	0.1	0.2	0.4	0.3	0.5	0.3
4-Methyl tridecane	22.27	0.2	0.2	0.2	0.3	0.1				0.2	0.2	0.2	0.1
Tetramethylsilane	23.16	3.7	8.3	7.8	12.4	2.4	1.1	2.0	2.2	5.8	8.7	12.6	6.4
4-methyl Undecane	23.48	0.1	0.1		0.2					0.1		0.1	
2-Methyl tridecane	23.60	0.1	0.0	0.1	0.4	0.0				0.2		0.1	0.0
2,6-Dimethyl undecane	24.00	0.1	0.1		0.3					0.1			
Total		208.3	98.1	97.7	211.8	263.2	45.7	112.3	33.7	280.1	110.6	141.8	94.5

The top five VOCs at the four altitudes had the following order from highest to lowest: site 1, 2,4-dimethyl heptane > toluene > propyl propionate > 3,7-dimethyl undecane > tetramethylsilane; site 2, propyl propionate > 2,4-dimethyl heptane > toluene > 2-methyl pentane > hexamethylcyclotrisiloxane; and site 3, 2,4-dimethyl heptane > toluene > propyl propionate > 2-methyl pentane > tetramethylsilane. The ranges of the concentration ratios of the top five species to all the upper-altitude VOCs at sites 1, 2, and 3 were 56.0%–68.5% (average = 61.5%), 51.7%–72.6% (average = 60.1%), and 54.1%–67.9% (average = 59.5%), respectively. The predominance of the top five species in the total upper-altitude VOC concentration in field measurement 2 was lower than that in field measurement 1, which was because more VOCs were detected in field measurement 2 than in field measurement 1.

2,4-Dimethyl heptane and toluene had the highest and second-highest concentrations among the VOCs at sites 1 and 3, respectively. However, at site 2, they had the second- and third-highest concentrations, respectively, with propyl propionate having the highest concentration. Toluene is the most common organic compound and originates from vehicle exhaust and industrial emissions. At each site, the detected concentrations of industrial organic solvents, such as benzene, xylene, ethylbenzene, butanone, acetone, isopropyl alcohol, and ethyl acetate, were higher in field measurement 2 than in field measurement 1. Isopropyl alcohol is a crucial cleaning agent and disinfectant in high-tech factories. The second largest high-tech park in Taiwan is located approximately 4 km north of the study area. Thus, a considerable quantity of the toluene detected in field measurement 2 originated from industrial emissions. 2,4-Dimethylheptane is a crucial component of high-octane fuel, such as gasoline; thus, the detected 2,4-dimethylheptane content mainly originated from vehicle emissions. Hexamethylcyclotrisiloxane is used as an additive in the creation of plastic and rubber products, paints, adhesives, cosmetics, food packaging, and many other products; thus, the detected hexamethylcyclotrisiloxane content probably originated from TIP and TPMP (Fig. 4). Tetramethylsilane is used as a starting material for synthesizing more complex organosilanes, and the tetramethylsilane detected in field measurement 2 might have also originated from TIP and TPMP. In addition, propyl propionate is a safer substitute for toluene because of its low odor, moderately volatile nature, and nonhazardous and nonpolluting ester product; thus, the propyl propionate detected in field measurement 2 mainly originated from industrial emissions. Alkanes were the dominant VOCs at various altitudes and sites in field measurement 2. Thus, concentrations of the VOCs originating from vehicle exhaust might have been higher than those of the VOCs originating from industrial exhaust, which is in line with the results of field measurement 1. The order of average VOC concentrations at the three sites in field measurement 2 was as follows: site 3 > site 1 > site 2. This order differed from that in field measurement 1, and this difference was probably because the prevailing winds in the study area changed from north–northeast in field measurement 1 to northeast by east in field measurement 2.

4 Discussion

In this study, a UAV platform with sensing and sampling systems was developed for 3D air pollutant concentration measurements. This platform was used in two measurement periods for detecting air pollutant concentrations in a large special industrial zone that includes a traditional industrial park, a precision machinery park, and a municipal waste incineration plant. To elucidate the transport of air pollutants in the aforementioned industrial zone, this study used a single theodolite on the ground to measure the speeds and directions of the upper winds during the field measurement periods. The use of this method prevented the airflow caused by the rotor of the UAV from influencing the measurements. The measurement results obtained by the sensing system of the developed platform, which contains multiple microsensors and is integrated with IoT technology, demonstrated the feasibility of this platform for determining the real-time 3D distributions of critical air pollutants. The NO_2 and O_3 contents were 0 ppm in the two field measurements because the sensitivities of the NO_2 and O_3 sensors were too low. All VOC concentrations at the three field measurement sites were very low (≤0.02 ppm), possibly because the sensitivity of the VOC sensor was also too low. The sum of the O_3 and NO_2 concentrations ($[O_3] + [NO_2]$) is defined as odd oxygen (ODO) in atmospheric chemistry (Yee et al., 2021; Zhang et al., 2018). Many studies have indicated that a high positive correlation exists between the concentrations of ODO and secondary organic aerosols (SOA's) (Hernod et al., 2008; Wood et al., 2010; Hu et al., 2016); thus, the concentration of SOA can be represented by the sum of the O_3 and NO_2 concentrations. SOA can have detrimental effects on the health and mortality of patients with chronic inflammatory diseases (Déméautis et al., 2022). Therefore, developing highly sensitive O_3, NO_2, and VOC microsensors is desirable for improving UAV air pollutant telemetry.

The sampling system of the developed platform, which contains multiple remote-controllable gas sampling sets, can conduct multipoint sampling according to the relevant situation for analyzing the composition of air pollutants. The results show that it is feasible to replace a canister with the sampling bag 1-L Tedlar bag for the 3D measurement of VOC concentrations according to the procedures of the TO-15 method of the US EPA. Moreover, the three air pumps of the gas sampling kits are connected in parallel to a length of 60-cm vertical sampling tube at the top of the UAV. The sampling tube was at the top of the UAV because the propeller causes downwash when UAV is close to the ground (Yang et al., 2020). In addition, the dispersion effects of drone propellers are small in the monitoring of atmospheric pollutants (Fan et al., 2023) but cause a large negative bias in the measurement of pollutant concentrations in plumes. (Villa et al., 2016). Therefore, the arrangement of the vertical sampling pipe is acceptable.

The observation and analysis data obtained from the single-theodolite method, sensing system, and sampling system were used to examine the effect of air pollutant discharge from the investigated industrial zone on the study area. The results of this study indicate the feasibility of using the developed UAV platform to accurately identify pollutants and determine their 3D spatial distributions concentrations in a study area. Thus, the UAV platform can serve as a useful tool in the management and decision-making process of air pollution in industrial areas.

5 Conclusions

Most research on the application of UAV systems in air pollution monitoring has focused on the development of microsensors and control and communication systems; few studies have used UAV systems for the sampling and analysis of low-altitude pollutants near the ground level. Therefore, in the present study, a UAV platform with sensing and sampling systems was developed for 3D air pollutant concentration measurements. The sensing system of this platform contains multiple microsensors and IoT technologies for obtaining the real-time 3D distributions of critical air pollutants. The sampling system contains multiple remote-controllable gas sampling sets as sampling devices, and these sampling sets contain a 1-L Tedlar bag instead of a canister for the 3D measurement of VOC concentrations in accordance with the TO-15 method of the US EPA. The developed platform was used to detecting air pollutant emissions in a large special industrial zone that includes a traditional industrial park, precision machinery park, and municipal waste incineration plant. According to the local prevailing wind direction in the study area, three field measurement sites were selected—one site located upwind and two sites located downwind. Comprehensive air pollutant characterization was performed in the aforementioned industrial zone during two field measurements in March and May 2023. The results of this characterization indicate that the developed UAV platform can accurately obtain the 3D concentration distributions of critical air pollutants in real time and conduct multipoint sampling according to the relevant situation for analyzing the composition of air pollutants.

Data availability. Data not available - participant consent.

Author contributions. JWL developed the concept and methodology for this work. JWL and CHS processed the field measurements data collected, and analysis of the samples. JWL provided scientific expertise on in situ data. Data handling and analysis were performed by CHS with contributions from JWL. All authors contributed to the proofreading and added valuable suggestions to the final draft.

Competing interests. The contact author has declared that none of the authors has any competing interests.

Acknowledgments. The authors gratefully acknowledgments distinguished Professor Jeng-Jong Liang, Feng Chia University, Taiwan, for providing the air pollution expertise and using his gas chromatography/mass spectrometry; and like to thank Green Ideas Synergy Co., Taiwan, for providing the micro sensors and using company's IoT framework for this research.

Financial support. This research has been supported by the Taichung City Environmental Protection Bureau, Taiwan, for financially supporting this research under Taichung EPB-P1111017073.

References

Alvarado, M., Gonzalez, F., Fletcher, A., Doshi, A.: Towards the development of a low cost airborne sensing system to monitor dust particles after blasting at open-pit mine sites. Sensors 15, 19667−19687, https://doi.org/10.3390/s150819667, 2015.

Arroyo, P., Gómez-Suárez, J., Herrero, J. L., Lozano, J.: Electrochemical gas sensing module combined with Unmanned Aerial Vehicles for air quality monitoring. Sens. Actuators B. Chem. 364, 131815, https://doi.org/10.1016/j.snb.2022.131815, 2022.

Boursianis, A. D., Papadopoulou, M. S., P. Diamantoulakis, et al.: Internet of Things (IoT) and Agricultural Unmanned Aerial Vehicles (UAVs) in smart farming: A comprehensive review. Internet of Things 18, 100187, https://doi.org/10.1016/j.iot.2020.100187, 2022.

Cozma, A., Firculescu, A. C., Tudose, D., Ruse, L.: Autonomous multi-rotor aerial platform for air pollution monitoring. Sensors 22(3), 860, https://doi.org/10.3390/s22030860, 2022.

De Fazio, R., Matteo Dinoi, L., De Vittorio, M., Visconti, P.: A sensor-based drone for pollutants detection in Eco-Friendly Cities: Hardware design and data analysis application. Electronics 11, 52, https://doi.org/10.3390/electronics11010052, 2022.

Déméautis, T., Delles, M., Tomaz, S., Monneret, G., Glehen, O., Devouassoux, G., George, C., Bentaher, A.: Pathogenic mechanisms of secondary organic aerosols. Chem. Res. Toxicol. 35(7), 1146–1161, ttps://doi.org/10.1021/acs.chemrestox.1c00353, 2022.

Duangsuwan, S., Prapruetdee, P., Subongkod, M., Klubsuwan, K.: 3D AQI mapping data assessment of low-altitude drone real-time air pollution monitoring. Drones 6, 191, https://doi.org/10.3390/drones6080191, 2022.

Fan, G., Liu, Z., Qin, Y., Long, B., Li, H., Li, J.: Airflow characteristics of rotorcraft plant protection UAV operating in rice fields. Biosyst. Eng. 226, 209–222, https://doi.org/10.1016/j.biosystemseng.2023.01.007, 2023.

Fumian, F., Chierici, A., Bianchelli, M., Martellucci, L., Rossi, R., Malizia, A., Gaudio, P., d'Errico, F., Giovanni D.D.: Development and performance testing of a miniaturized multi-sensor system combining MOX and PID for potential UAV application in TIC, VOC and CWA dispersion scenarios. Eur. Phys. J. Plus 136, 913, https://doi.org/10.1140/epjp/s13360-021-01858-2, 2021.

Fumian, F., Giovanni, D.D., Martellucci, L., Rossi, R., Gaudio, P.: Application of miniaturized sensors to unmanned aerial systems, a new pathway for the survey of polluted areas: preliminary results. Atmosphere 11, 471, https://doi.org/10.3390/atmos11050471, 2020.

Galle, B., Arellano, S., Bobrowski, N., et. al.: A multi-purpose, multi-rotor drone system for long-range and high-altitude volcanic gas plume measurements. Atmos. Meas. Tech. 14, 4255–4277, https://doi.org/10.5194/amt-14-4255-2021, 2021.

Gu, Q., Jia, C.: A consumer UAV-based air quality monitoring system for smart cities. 2019 IEEE International Conference on Consumer Electronics (ICCE), DOI: 10.1109/ICCE.2019.8662050, 2019.

Gu, Q., Michanowicz, D. R., Jia, C.: Developing a modular unmanned aerial vehicle (UAV) platform for air pollution profiling. Sensors 18, 4363, https://doi.org/10.3390/s18124363, 2018.

Herndon, S. C., Onasch, T. B., Wood, E. C., Kroll, J. H., et al.: Correlation of secondary organic aerosol with odd oxygen in Mexico City. Geophys. Res. Lett. 35, 15804, doi:10.1029/2008GL034058, 2008.

Hu, W., Hu, M., Hu, W., Jimenez, J. L., Yuan, B., Chen, W., et al.: Chemical composition, sources, and aging process of submicron aerosols in Beijing: Contrast between summer and winter. J. Geophys. Res. Atmos. 121 (2016) 1955–1977, https://doi.org/10.1002/2015JD024020, 2016.

Huang, F., Peng, S., Yang, H., Cao, H., Ma, N., Ma, L.: Development of a novel and fast XRF instrument for large area heavy metal detection integrated with UAV. Environ. Res. 214, 113841, https://doi.org/10.1016/j.envres.2022.113841, 2022.

Leitner, S., Feichtinger, W., Mayer, S., Mayer, F., Krompetz, D., Hood-Nowotny, R., Watzinger, A.: UAV-based sampling systems to analyse greenhouse gases and volatile organic compounds encompassing compound-specific stable isotope analysis. Atmos. Meas. Tech., 16, 513–527 https://doi.org/10.5194/amt-16-513-2023, 2023.

Liu, C., Huang, J., Wang, Y., Tao, X., Hu, C., Deng, L., Xu, J., Xiao, H. W., Luo, L., Xiao, H. Y., Xiao, W.: Vertical distribution of $PM_{2.5}$ and interactions with the atmospheric boundary layer during the development stage of a heavy haze pollution event. Sci. Total Environ. 704, 135329, https://doi.org/10.1016/j.scitotenv.2019.135329, 2020.

Middleton, W. E. K., Spilhaus A. F.: Meteorological Instruments. 3rd ed., Heritage: University of Toronto Press. pp181-183. doi.org/10.3138/9781487572013-056, 2019.

Noori, R., Dahnil, D. P.: The effects of speed and altitude on wireless air pollution measurements using hexacopter drone. (IJACSA) Int. J. Adv. Comput. Sci. Appl. 11(9), 268-276, (DOI): 10.14569/IJACSA.2020.0110931, 2020.

Pochwała, S., Gardecki, A., Lewandowski, P., Somogyi, V., Anweiler, S.: Developing of low-cost air pollution sensor—Measurements with the unmanned aerial vehicles in Poland. Sensors 20, 3582, https://doi.org/10.3390/s20123582, 2020.

Pounds, P.E.I., Bersak, D.R., Dollar, A.M.: Grasping from the air: Hovering capture and load stability. 2011 IEEE ICRA SHICC, May, 2011, Shanghai, China. DOI: 10.1109/ICRA.2011.5980314, 2011.

Qiu, S., Chen, B., Wang, R., Zhu, Z., Wang, Y., Qiu, X.: Estimating contaminant source in chemical industry park using UAV-based monitoring platform, artificial neural network and atmospheric dispersion simulation. RSC Adv. 7, 39726–39738, https://doi.org/10.1039/C7RA05637K, 2017.

Samad, A., Florez, D.A., Chourdakis, I., Vogt, U.: Concept of using an unmanned aerial vehicle (UAV) for 3D investigation of air quality in the atmosphere—Example of measurements near a roadside. Atmosphere 13, 663, https://doi.org/10.3390/atmos13050663, 2022.

Shen, L., Cheng, Y., Bai, X., Dai, H., et al.: Vertical profile of aerosol number size distribution during a haze pollution episode in Hefei, China. Sci. Total Environ. 814, 152693, https://doi.org/10.1016/j.scitotenv.2021.152693, 2022.

Singh, P. K., Sharma, A.: An intelligent WSN-UAV-based IoT framework for precision agriculture application. Comput. Electr. Eng. 100, 107912, https://doi.org/10.1016/j.compeleceng.2022.107912. 2022.

Sun, X., Zhao, T., Tang, G., Bai, Y., et al.: Vertical changes of $PM_{2.5}$ driven by meteorology in the atmospheric boundary layer during a heavy air pollution event in central China. Sci. Total Environ. 858, 159830, https://doi.org/10.1016/j.scitotenv.2022.159830, 2023.

Suroto, A., Ubaidillah, A., Ulum, M.: Air condition monitoring using way point based UAV (Unmanned Aerial Vehicle). Int. J. Sci. Eng. Inf. Technol. 3(1), 109−114, https://journal.trunojoyo.ac.id/ijseit, 2018.

Yang, S., Tang, Q., Zheng, Y., Liu, X., Chen, J.,ation of a six-rotor UAV downwash,» Int. J. Agric.

Biol. Eng.13(4),10–18, 2020

Villa, T. F., Salimi, F., Morton, K., Morawska, L., Gonzalez, F.: Development and validation of a UAV based system for air pollution measurements. Sensors 16, 2202, https://doi.org/10.3390/s16122202, 2016.

Wood, E. C., Canagaratna, M. R., Herndon, S. C., et al.: Investigation of the correlation between odd oxygen and secondary organic aerosol in Mexico City and Houston. Atmos. Chem. Phys. Discuss. 10 (2010) 8947–8968, https://doi.org/10.5194/acp-10-8947-2010, 2010.

Xie, T., Liu, R., Hai, R. T., Hu, Q. H., Lu. Q.: UAV platform based atmospheric environmental emergency monitoring system design. J. Appl. Sci. 13(8), 1289–1296, https://doi: 10.3923/jas.2013.1289.1296, 2013.

Yang, S., Tang, Q., Zheng, Y., Liu, X., Chen, J., Li, X.: Model migration for CFD and verification of a six-rotor UAV downwash. Int. J. Agric. Biol. Eng.13(4) 10–18, DOI: 10.25165/j.ijabe.20201304.5569, 2020.

Yang, Z., Yu, X., Dedman, S., Rosso, M., Zhu, J., Yang, J., Xia, Y., Tian, Y., Zhang, G., Wang, J.: UAV remote sensing applications in marine monitoring: Knowledge visualization and review. Sci. Total Environ. 838, 155939, https://doi.org/10.1016/j.scitotenv.2022.155939, 2022.

Yee, L. D., Craven, J. S., Loza, C. L., Schilling, K. A., Ng, N. L., et al.: Secondary organic aerosol formation from low-NOx photooxidation of dodecane: evolution of multigeneration gas-phase chemistry and aerosol composition, J. Phys. Chem. A 116(24), 6211–6230, https://doi.org/10.1021/jp211531h, 2021.

Yee, L., Pollak, W., Brunt, D., et al.: A new theodolite for following fast moving objects especially for making pilot balloon observations of greater accuracy. Q. J. R. Meteorol. Soc. 65, 443−447, https://doi.org/10.1002/qj.49706528117, 1939.

Yungaicela-Naula, N. M., Garza-Castaňón, L. E., Mendoza-Domínguez, A., Minchala-Avila, L. I., Garza-Elizondo, L. E.: Design and implementation of an UAV-based platform for air pollution monitoring and source identification. 2017 Congreso Nacional de Control Automático, Monterrey, Nuevo León, Mexico. https://amca.mx/memorias/amca2017/media/files/0041.pdf, 2017.

Zhang, C., Lu, X. H., Zhai, J. H., Chen, H., Yang, X., Zhang, Q., et al.: Insights into the formation of secondary organic carbon in the summertime in urban Shanghai. J Environ Sci -China. 72, 118–132, https://doi.org/10.1016/j.jes.2017.12.018, 2018.

Zheng, T., Li, B., Li, X. B., Wang, Z., Li, S. Y., Peng, Z. R.: Vertical and horizontal distributions of traffic-related pollutants beside an urban arterial road based on unmanned aerial vehicle observations. Build. Environ. 187, 107401, https://doi.org/10.1016/j.buildenv.2020.107401, 2021.

Zhu, X., Zhu, X., Rui Yan, R., Peng R.: Optimal routing, aborting and hitting strategies of UAVs executing hitting the targets considering the defense range of targets. Reliab. Eng. Syst. Saf. 215, 107811, https://doi.org/10.1016/j.ress.2021, 2021.